Fuel 346 (2023) 128298

Contents lists available at ScienceDirect

Fuel

journal homepage: www.elsevier.com/locate/fuel

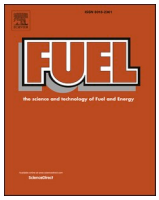

Full Length Article

Effect of water and methanol concentration in the feed on the deactivation of In_2O_3-ZrO_2/SAPO-34 catalyst in the conversion of CO_2/CO to olefins by hydrogenation

A. Portillo, O. Parra, J. Ereña, A.T. Aguayo, J. Bilbao, A. Ateka *

Department of Chemical Engineering, University of the Basque Country UPV/EHU, P.O. Box 644, 48080 Bilbao, Spain

ARTICLE INFO

Keywords:
CO_2 valorization
Olefins
SAPO-34
Tandem catalysts
Deactivation

ABSTRACT

On account of the superior performance of In_2O_3-ZrO_2/SAPO-34 tandem catalyst in the direct synthesis of olefins from CO, CO_2 and CO/CO_2 mixture by hydrogenation, it is interesting to establish the conditions to avoid its deactivation due to the rapid coke deposition on SAPO-34. The co-feeding of H_2O and/or methanol together with H_2 + CO_2/CO was studied in a packed bed reactor at: 400 °C, 30 bar; CO_2/CO_x in the feed, 0–1; H_2/CO_x in the feed, 1–3; and space time of 5 g_{cat} h mol_C^{-1}, quantifying the evolution with time on stream (up to 16 h) of CO_2 and CO_x conversions and olefin, paraffin and CH_4 yields. The effects of the co-feeding on coke content and its nature were determined by temperature programmed oxidation (TPO) analyses of the spent catalyst. The results highlighted the complex effect of the concentration of H_2O and oxygenates (methanol/dimethyl ether (DME)) on the deactivation of SAPO-34 and on the products yields in the pseudo-steady state of the catalyst. Co-feeding H_2O lessens coke deactivation, however, high H_2O concentration leads to attenuate the acidity of SAPO-34, limiting the performance of the tandem catalyst (mainly in the CO_2 conversion). Oxygenates co-feeding concentration limit value lies on its favoring effect for coke formation. In addition to this effect, the favorable attenuation of coke deactivation by the high H_2 concentration (studied in runs with H_2/CO_x ratio in the feed in the 1–3 range) plays a key role in the viability of the process, leading to a pseudo-steady catalyst state in which the activity is constant. The proven effect of H_2O and methanol concentrations will be useful for establishing new catalysts and reaction conditions at which their presence in the reactor will attenuate deactivation.

1. Introduction

In order to mitigate climate change, the carbon capture and utilization (CCU) technologies have received a great deal of attention, encouraging the valorization of CO_2 mainly through its transformation into chemicals and fuels [1–3]. Moreover, the joint valorization of CO_2 together with syngas is especially interesting when syngas (with CO and H_2 as main components) is obtained from sustainable routes such as biomass gasification or reforming of its derivatives [4–7]. In addition, with biosyngas co-feeding part of the needed H_2 is supplied.

Among the catalytic processes for CO and CO_2 hydrogenation, the direct synthesis of hydrocarbons offers the advantage of integrating in the same reactor the stages for CO/CO_2 hydrogenation and the conversion of the intermediates into the targeted hydrocarbon products such as fuels and chemicals. The extent of the conversion of the intermediates favors the displacement of the equilibrium of thermodynamically limited reactions, boosting the conversion of CO_2. This process can be carried out *via* the modified Fischer Tropsch synthesis or with methanol/dimethyl ether (DME) as intermediates. Tandem catalysts are used, combining metal oxides and acidic zeotypes for each reaction stage [8–10].

Not being limited by the Anderson-Shulz-Flory (ASF) distribution, the route with methanol/DME as intermediates is suitable for obtaining high olefin selectivity [11]. Guo et al. [12] studied the thermodynamics of the methanol synthesis stage, emphasizing the complex role of CO. Thus, in the CO_2 hydrogenation at equilibrium conditions, CO formation by the reverse WGS (rWGS) had a negative effect on the conversion of CO_2 and on methanol yield. Whereas co-feeding CO with CO_2 increased these equilibrium values. As these authors stated, the results obtained under favorable thermodynamic conditions will be conditioned by the activity and selectivity of the catalysts used, highlighting that the results in the methanol to olefins conversion stage are a direct consequence of

* Corresponding author.
E-mail address: ainara.ateka@ehu.eus (A. Ateka).

https://doi.org/10.1016/j.fuel.2023.128298
Received 30 January 2023; Received in revised form 27 March 2023; Accepted 31 March 2023
Available online 13 April 2023

the selectivity of the zeotype used in the tandem catalyst composed of a metallic oxide and acid zeotype (OX/ZEO tandem catalysts). The most studied catalysts are prepared mainly using oxides of In or Zn with ZrO_2 as promoter for methanol synthesis: ZnO-ZrO_2 [13–15], In_2O_3 [16–18], In_2O_3-ZrO_2 [19–21] or In_2O_3-ZnO-ZrO_2 [22]. These catalysts are more stable at the required operating temperature (≥300 °C for the oxygenate conversion into hydrocarbons) than the conventionally employed Cu-based catalysts [23]. The zeotype catalysts for the selective production of olefins are primarily based on the silicoaluminophosphate SAPO-34 [13,15,16,18–21,23], mainly thanks to its severe shape selectivity (with CHA structure). Among the attempts to improve the performance of SAPO-34 by modulating its acidity, the addition of HF during the synthesis was ascertained to provide more acid strength to the zeolite and boost light olefins selectivity using a GamCrOx/H-SAPO (F) tandem catalyst, while reducing CO selectivity [24]. Alternatively, for the production of higher hydrocarbons catalysts based on HZSM-5 zeolite (MFI structure) are applied, with lower severity of shape selectivity [14,17].

Even if the severe shape selectivity of the SAPO-34 catalyst is suitable for the selective production of light olefins, it is well established for the MTO/DTO processes that as a drawback it promotes the confinement of the coke precursor intermediates [25,26] and their evolution towards polyaromatic structures, which block the acid sites and the porous structure [27]. It is also remarkable the foreseeable autocatalytic nature of coke formation, whose rate in the MTO/DTO processes is dependent on the methanol/DME concentration [28]. Among the strategies to attenuate coke deactivation, the decrease of the crystal particle size and the hierarchical organization of the pore structure of the catalyst particle stand out [29]. The concentration of water has a favorable incidence on the attenuation of the deactivation [30,31], which motivates its co-feeding [32,33], although competition for the adsorption of water and methanol/DME and reaction intermediates in the acid sites also diminishes their activity for the production of olefins [34–36]. Moreover, the favorable contribution of the high H_2 partial pressure for attenuating coke deposition on methanol/DME conversion into hydrocarbons is noteworthy [37–39] due to the hydrogenation of the coke precursors [40]. Presumably, these effects will exist in the direct synthesis of olefins from CO_2/CO hydrogenation, although the conditions and the composition of the reaction medium are different. Hence, the presence of H_2 in the direct synthesis of olefins from CO_2/CO hydrogenation results in a lower deactivation of the SAPO-34 catalyst [41].

In a previous work [42], the optimal composition of the In_2O_3-ZrO_2 catalyst was determined (with an In/Zr ratio of 1/2), in order to favor the conversion of CO_2 and CO_x (CO_2/CO) mixtures. This way, the sintering of In by over-reduction was avoided, and the secondary methanation reaction was suppresed. In addition, the optimal conditions (moderate pressure of 30 bar, 400 °C, H_2/CO_x ratio in the feed of 3), suitable for obtaining with the In_2O_3-ZrO_2/SAPO-34 tandem catalyst a high per pass yield of olefins (greater than 4%) with a selectivity greater than 70 % being propylene the major olefin, were determined [41]. It should be pointed out that the catalyst undergoes a rapid initial deactivation, and subsequently reaches a pseudo-steady state of constant activity, in which coke formation rate is equal to its elimination rate by hydrogenation.

This work addresses the drawback of the deactivation of the In_2O_3-ZrO_2/SAPO-34 tandem catalyst, which conditions its feasibility for the direct synthesis of olefins from CO_2/CO feeds. The study emphasizes the effect of reaction conditions (H_2 partial pressure, water and methanol concentration in the reaction medium) that will have an impact on the coke deposition in SAPO-34 (origin of the deactivation). The results will be of interest to adapt the properties of the catalyst and operating conditions with the objective of lessening the deactivation.

2. Experimental

2.1. Catalyst synthesis and characterization

In_2O_3-ZrO_2 catalyst was synthesized following a co-precipitation method described in detail in a previous work [42]. Briefly, metallic nitrates ($In(NO_3)_3$ and $Zr(NO_3)_4$, Panreac) were dissolved in water (1 M) in a 2/1 In/Zr ratio and coprecipitated with $(NH_4)_2CO_3$ at 70 °C and maintaining the pH close to 7. Subsequently, the sample was dried, calcined and pelletized. The best configuration was ascertained to be the mixture of individually pelletized In_2O_3-ZrO_2 (125–250 μm) and SAPO-34 (300–400 μm) catalyst particles in a 2/1 mass ratio diluted in SiC [43]. The different particle size eases the separation of the individual spent catalysts by sieving in order to analyze them.

In_2O_3-ZrO_2 and SAPO-34 catalysts were characterized by N_2 adsorption–desorption analyses (Micromeritics ASAP 2010), NH_3-temperature programmed desorption (NH_3-TPD) analyses and H_2 and CO temperature programmed reduction (H_2-TPR and CO-TPR). Characterization results are shown in Table 1 (physical properties and acidity) and in Supporting Information (Fig. S1) (TPR analyses). The high value of the BET surface area of the SAPO-34 catalyst (651.8 $m^2\ g^{-1}$), consistet with its microporous structure, as well as its high acidity (777.6 $\mu mol_{NH3}\ g_{cat}^{-1}$) should be noted. The remarkable surface area of the In_2O_3-ZrO_2 catalyst is consequence of the mesoporous structure of both oxides. Thus, S_{BET} accounts for 53.4 $m^2\ g^{-1}$ for In_2O_3 and 95.4 $m^2\ g^{-1}$ for ZrO_2, and the pore volume 0.25 and 0.16 $cm^3\ g^{-1}$, respectively [42]. The acidity (122.6 $\mu mol_{NH3}\ g_{cat}^{-1}$) is attributable to ZrO_2. The results in Fig. S1 of In_2O_3-ZrO_2 catalyst TPR are in line with previous results [42], where the higher reducing capability of CO compared to H_2 is confirmed, in line with the literature [42,44,45].

2.2. Catalytic activity test

CO_2/CO hydrogenation reactions were carried out in a reaction equipment (PID End & Tech Microactivity Reference) described in previous works [42,46] equipped with an isothermal stainless steel packed bed reactor, with an effective length of 10 cm and an inner diameter of 9 mm and it can operate at conditions up to 800 °C and 100 bar. It is provided with an internal ceramic coating to avoid side reactions with the reactor walls. For each run the reactor was loaded with a mixture of the desired catalyst amount and SiC (up to 5 g of solid mixture) to avoid preferential pathways, ensure isothermal conditions and sufficient bed-height when using small space time values. In order to analyze the products on-line, a representative fraction of the reactor outlet stream was diluted in He and sent to an on-line connected gas chromatograph (Varian CP-4900). The microGC is equipped with MS-5, Porapak Q and CPSiL columns, allowing the quantification of compounds comprising H_2, H_2O, oxygenates (methanol and DME) and hydrocarbons up to C_9.

The coke deposited over the spent catalysts was studied by temperature programmed oxidation (TPO) analyses (TA Instruments TGA Q5000 thermobalance), consisting of: i) sweeping of the sample with He at 120 °C for 30 min to remove the humidity, ii) stabilizing of the sample in air at 120 °C (10 $cm^3\ min^{-1}$) and iii) heating of the sample up to 680 °C with a heating rate of 7 °C min^{-1}. The weight of the sample was measured during the whole experiment to ascertain that all humidity

Table 1
Physical and acid properties of the metallic and acid catalysts.

Catalyst	S_{BET} ($m^2\ g^{-1}$)	$V_{micropore}$ ($cm^3\ g^{-1}$)	V_{pore} ($cm^3\ g^{-1}$)	d_p (nm)	Acidity ($\mu mol_{NH3}\ g_{cat}^{-1}$)
In_2O_3-ZrO_2	86	0.003	0.23	9.0	122.6
SAPO-34	652	0.219	0.23	1.5	777.6

was desorbed during the first step.

The reaction runs were carried out under the following conditions: 350–425 °C; 20–50 bar; space time, 5 g_{cat} h mol_C^{-1}; H_2/CO_x, 1–3; H_2/CO_x, 0–1. The effect of H_2O and methanol content in the reaction medium was studied co-feeding both in a 5 % molar fraction.

The results were quantified from the molar flows at the inlet and outlet of the reactor in contained C units, as follows.

Conversion of CO_2 (X_{CO2}):

$$X_{CO_2} = \frac{F^0_{CO_2} - F_{CO_2}}{F^0_{CO_2}} 100 \quad (1)$$

where F^0_{CO2} and F_{CO2} are the CO_2 molar flowrates at the inlet and outlet of the reactor, respectively.

The conversion of the CO and CO_2 mixture (the carbon fraction converted into hydrocarbons or oxygenates) (X_{COx}) was defined as:

$$X_{CO_x} = \frac{F^0_{CO_x} - F_{CO_x}}{F^0_{CO_x}} 100 \quad (2)$$

where F^0_{COx} is inlet molar flowrate in C atoms, and F_{COx} its analogous at the outlet of the reactor.

Carbonaceous product yields (Y_i) and selectivities (S_i) were defined by grouping the products in lumps: CH_4, C_2-C_4 olefins, C_2-C_4 paraffins and oxygenates (methanol and DME) according to the following expressions:

$$Y_i = \frac{n_i F_i}{F^0_{CO_x}} 100 \quad (3)$$

$$S_i = \frac{n_i F_i}{\sum n_i F_i} 100 \quad (4)$$

being n_i the number of C atoms in a molecule of *i* component (or lump) and F_i the corresponding molar flowrate at the reactor outlet stream.

3. Results

3.1. Coke deposition over SAPO-34

Fig. 1 shows the TPO profiles of the two individual catalysts after a certain reaction. It is evident that most of the coke was formed over SAPO-34 (where coke amount accounted up to 10.9 wt% while in In_2O_3-ZrO_2 did not reach 0.6 wt%). The high coke content for SAPO-34 is typical of the MTO/DTO processes [26,47–49] and it is explained by the confinement capacity of the intermediate arenes formed in the dual cycle mechanism in the cages of SAPO-34 catalyst. The wide

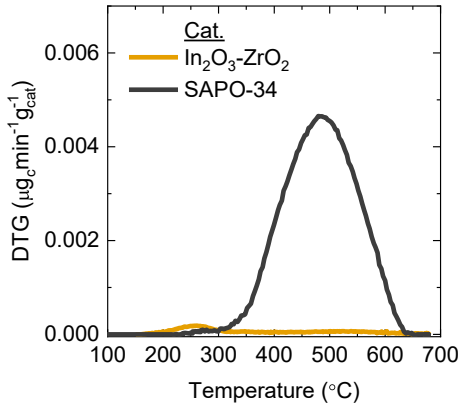

Fig. 1. Comparison of TPO profiles for the individual In_2O_3-ZrO_2 and SAPO-34 spent catalysts. Reaction conditions: 400 °C; 30 bar; CO_2/CO_x, 0.5; space time, 5 g_{cat} h mol_C^{-1}; H_2/CO_x, 3, and; time on stream, 16 h.

temperature range (250–650 °C) of the TPO profile corresponds to a coke formed by heterogeneous carbonaceous species, whose condensation towards polyaromatic structures during the reaction and its combustion in the TPO analysis will be limited by the diffusional restrictions in the cages of the SAPO-34. On the contrary, The hydrogenation capability of the In_2O_3-ZrO_2 catalyst enables the hydrogenation of coke precursors during the reaction and its mesoporous structure eases its diffusion outwards the catalyst particle, explaining its low content in 16 h on stream. Furthermore, in Fig. 1, the maximum combustion peak is observed at 450 °C for SAPO-34 and 270 °C for In_2O_3-ZrO_2, as the combustion of the coke deposited on the metallic oxides is catalyzed (which is interesting to facilitate its regeneration). In all the studied reaction conditions similar results to these plotted in Fig. 1 were obtained, pointing to coke formation over SAPO-34 as the main responsible of the deactivation of In_2O_3-ZrO_2/SAPO-34 tandem catalyst. Consequently, the same species that deactivate SAPO-34 during the MTO/DTO reactions will presumably be the reason for the deactivation of the tandem catalyst in the direct CO/CO_2 to olefins conversion too, as will be discussed below.

3.2. Effect of the feed composition

3.2.1. Water and methanol co-feeding with H_2/CO and H_2/CO_2 feeds

Various runs, where H_2O, methanol, and an equimolar mixture of H_2O and methanol were added to the H_2 + CO/CO_2 feed, were conducted to assess the role of H_2O and methanol intermediates in the direct hydrogenation of CO/CO_2 to olefins over the tandem catalysts. The H_2O flow rate fed was calculated to simulate the same concentration as that generated stoichiometrically by the rWGS reaction with H_2/CO_2 feeds, which corresponds to approximately 5 mol%. Consequently, the effect of CO and CO_2 can be compared as in all cases H_2O concentration was similar. For the co-feeding of methanol, the CO and CO_2 flow rates were adjusted to keep the same space time value. H_2/CO_x ratio in the feed was 3 in all runs.

In Fig. 2 product yields evolution with time on stream with H_2/CO feed is depicted together with the results obtained co-feeding H_2O and methanol. With the H_2/CO feed (Fig. 2a), the initial deactivation of SAPO-34 was very fast, which caused a decrease in olefin and paraffin (formed by hydrogenation of the former) yields, and led to an increase of the concentration of oxygenates (non converted) and CH_4 (formed by oxygenates cracking). These yields reached a constant value after 4 h on stream corresponding to the catalyst remaining activity.

H_2O co-feeding (Fig. 2b) attenuated the deactivation rate, delaying the time for acquiring a pseudo-steady state of the catalyst (up to 8 h) in which olefin and paraffin yields were similar to those obtained without H_2O in the feed. The higher yield of oxygenates and lower CH_4 yield demonstrate the effect of H_2O to attenuate the activity of SAPO-34 acid sites for the dual cycle mechanism and also for methanol/DME cracking [50,51]. Consequently, besides the lower deactivation, the smaller CH_4 yield is another interesting result that facilitates the recirculation of the products stream and helps to obtain higher conversion.

On the other hand, methanol co-feeding (Fig. 2c), did not lead to a higher olefin yield. Because the deactivation rate is directly dependent to oxygenates concentration. Thus, the yield of olefins and paraffins was stable after 2 h on stream and the values were significantly lower than at previous conditions. In this reached catalyst state, the oxygenate stream was mainly formed by DME, because methanol dehydration activity was maintained, which only required a low density of acid sites of reduced acid strength [35,52]. The high CH_4 yield obtained when co-feeding methanol suggests that CH_4 was being formed due to the high oxygenates (methanol and DME) partial pressure, which underwent thermal cracking at 400 °C (mainly DME as it is less stable than methanol) [53]. Thus, it is observed that an excessive formation of oxygenates has the drawback of strongly favoring the fast deactivation of SAPO-34 catalyst by coke. Based on the results, the incidence of H_2O co-feeding on the deactivation of the SAPO-34 catalyst was similar to the well-established

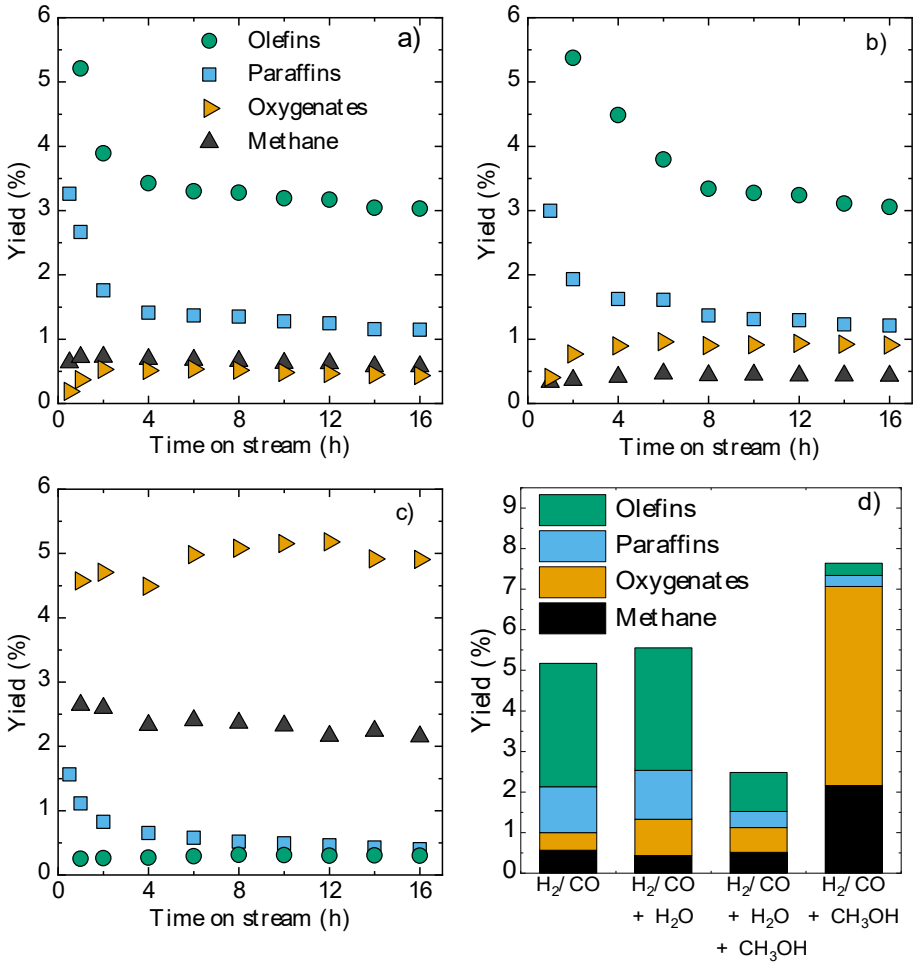

Fig. 2. Evolution of product yields with time on stream for H_2/CO feed without any co-feeding (a), co-feeding H_2O (b), cofeeding methanol (c), and their values at the pseudo-steady state of the catalyst (16 h on stream) (d). Reaction conditions: 400 °C; 30 bar; CO_2/CO_x, 0; space time, 5 g_{cat} h mol_C^{-1}, and; H_2/CO_x, 3.

effect on the conversion of methanol/DME to olefins (processes at atmospheric pressure and without H_2 presence). H_2O decreases the activity and attenuates the deactivation of the catalyst, as it competes for the adsorption in the acid sites with reactants and coke precursors [51,52]. It is also well-established for the methanol/DME conversion to olefins over different acid catalysts that increasing the concentration of reactant oxygenates results in a higher coking rate [33,53].

In terms of scaling up, it is interesting to compare the yields in the pseudo-steady state of the catalyst for the different feeds (Fig. 2d). When co-feeding H_2O, olefin yield in the pseudo-steady state of the catalyst was equal (and it was even higher before reaching this state, compared to pure H_2/CO feeds) and higher oxygenate yield was achieved. The latter occurs due to the shift of the equilibrium of the methanol to DME dehydration step (hampered by H_2O), which results in higher methanol yield in the medium and lower CH_4, enlightening that it is formed preferentially from DME thermal cracking. These effects (derived from the presence of H_2O) would take place without H_2O co-feeding when modifying many other process conditions, considering that H_2O is the product of numerous reactions of the direct CO_2/CO to olefins process: i) rWGS reaction, ii) synthesis of methanol from CO_2, iii) methanol dehydration to DME and iv) conversion of oxygenates to olefins.

The effect of methanol co-feeding in Fig. 2d shows a high oxygenate yield and CH_4. It is remarkable that DME is the major compound within the oxygenates (96 %). This occurs due to the fast deactivation of SAPO-34 catalyst, only capable of dehydrating methanol. Moreover, the low remaining activity of SAPO-34 for the conversion of methanol/DME *via* the dual cycle mechanism favors the CH_4 formation by DME thermal cracking. Consequently, this effect must be taken into account, operating under conditions in which the excess of oxygenates in the reaction medium is avoided.

Fig. 2d also gathers the results obtained with the catalyst in the pseudo-steady state with the joint co-feeding of H_2O and methanol. In this case, the excess of both components in the reaction medium combined their negative effects, resulting in a decrease in olefin yield and in an increase of DME yield. The CH_4 yield attained was similar to that obtained without co-feeding H_2O or methanol, suggesting that the effects of co-feeding methanol (favoring CH_4 formation) and H_2O (attenuating CH_4 formation) were compensated.

The effect of the co-feeding of H_2O and methanol was also evaluated for H_2/CO_2 feed (Fig. 3), comparing the results with the aforementioned for H_2/CO feed. As observed previously in Fig. 2b with H_2/CO feed, H_2O co-feeding led to a very even evolution of products distribution with time on stream (Fig. 3b) compared to the run without H_2O co-feeding (Fig. 3a). However, the conversion into olefins was strongly penalized by the thermodynamic effects (attenuation of the extent of rWGS, methanol formation, DME formation and MTO/DTO reactions). The results obtained by methanol addition (Fig. 3c) resulted in an excess of oxygenates that turned into a high CH_4 formation by DME (main oxygenate in this case) thermal cracking.

Comparing the product yields in the pseudo-steady state of the catalyst (Fig. 3d), it is observed that H_2O co-feeding also entailed a negative effect, in contrast to that observed for H_2/CO feed (Fig. 2d). This occurs because for H_2/CO_2 feed the rWGS reaction is favored and, thus, the H_2O generated by rWGS is added to the fed H_2O, resulting in an

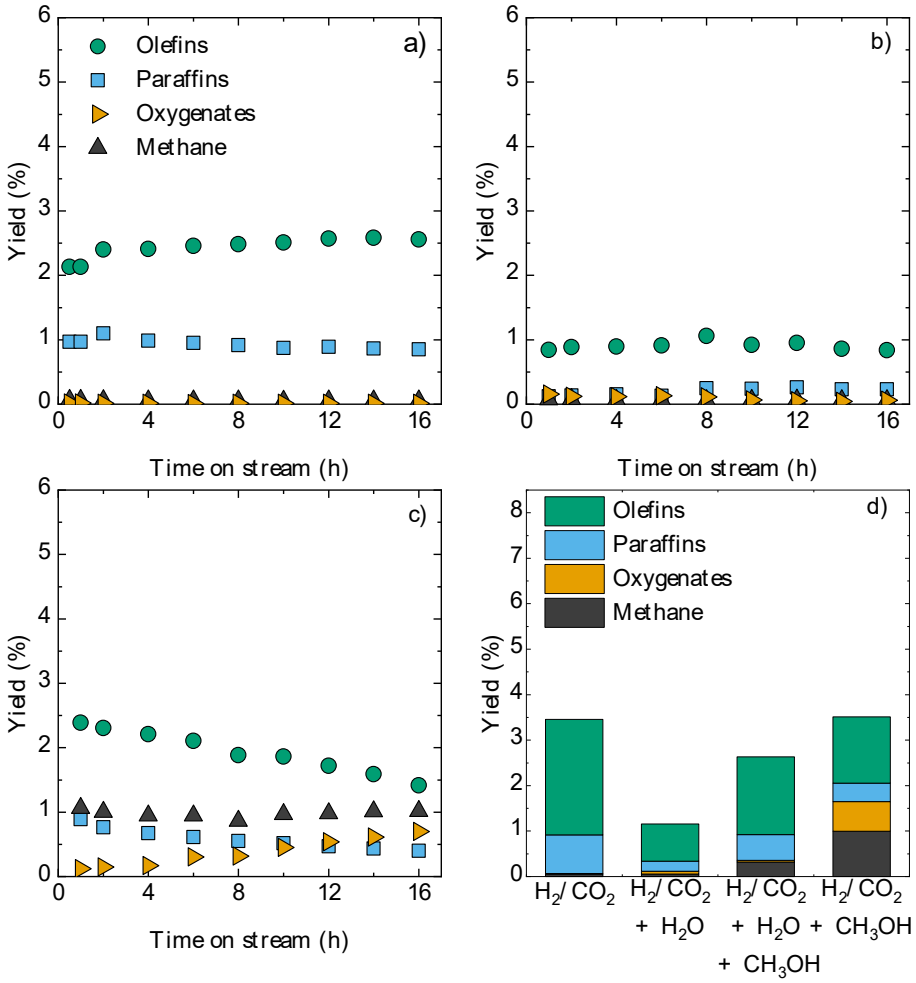

Fig. 3. Evolution of products yield with time on stream for H_2/CO_2 feed (a), with water co-feeding (b), with methanol co-feeding (c) and their values at pseudo-steady state of the catalyst (16 h on stream) (d). Reaction conditions: 400 °C; 30 bar; CO_2/CO_x, 1; H_2/CO_x, 3, and; space time, 5 g_{cat} h mol_C^{-1}.

excess of H_2O in the medium. Therefore, the high H_2O concentration excessively attenuated the extent of the dual cycle mechanism for olefin formation. On the other hand, analogously to what was observed for the H_2/CO feed, co-feeding methanol occasioned negative effects. CH_4 and DME were formed and olefin yield was lower. Furthermore, the joint co-feeding of H_2O and methanol integrated the negative effects. These results ratify the importance of H_2O and methanol/DME concentrations on the mechanisms of the direct synthesis of olefins from CO_2 and on deactivation. It is also noteworthy that the presence of H_2O in a small concentration had the positive effect of attenuating the deactivation with the H_2/CO feed. Nonetheless, an excessive H_2O concentration with H_2/CO_2 feed involved the negative effect of limiting the activity of the acid sites of SAPO-34 to be predominant.

All these effects over the catalyst deactivation are related to the differences in coke formation on the SAPO-34 catalyst. These trends are clearly observed in the TPOs gathered in Fig. 4 corresponding to the runs with H_2/CO_2 feed, without and with co-feeding H_2O, methanol and a mixture of both. On the one hand, co-feeding H_2O lessened coke content from 10.3 wt% to 4.3 wt%. Consequently, the noticeable limited activity of SAPO-34 observed in Fig. 3b and 3d is explained by the competence of H_2O with the oxygenates for its adsorption in the acid sites [51,52].

On the other hand, coke content rose up to 14.4 wt% when methanol was co-fed. Moreover, in this case, TPO profile was displaced to higher temperature (the corresponding to the highest combustion peak rate is at 500 °C), which is in line with a more condensed coke [30,40]. This takes place due to the higher extent of the condensation reactions of the

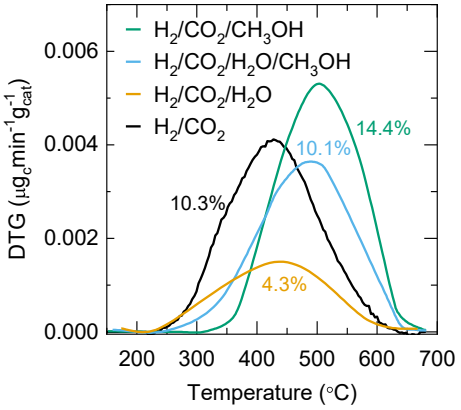

Fig. 4. Effect of the different co-feedings on the SAPO-34 TPO profiles and their corresponding coke content (wt%). Reaction conditions: 400 °C; 30 bar; CO_2/CO_x, 1; space time, 5 g_{cat} h mol_C^{-1}; H_2/CO_x, 3; and time on stream, 16 h.

arenes retained in the cages of SAPO-34, that will evolve into poly-aromatic condensed structures (coke with a lower H/C ratio). The joint co-feeding of H_2O and methanol resulted in an intermediate coke profile (compared to the two individual feeds), both in area (coke content 10.1 wt%) and position (combustion rate peak slightly lower than 500 °C), even if the negative effect of increasing methanol concentration was

predominant, favoring coke deposition and condensation. On the other hand, the symmetry of the TPO profiles hampers the identification of different coke types by deconvolution, which is indicative of the coke being deposited in a porous structure with uniform spaces (CHA topology with 10 × 6.7 cavities Å connected by 3.8 × 3.8 Å 8-ring cages) [54]. The long reaction time (16 h) contributes to the uniformity of the coke, since for all the conditions studied, the catalyst had already reached a pseudo-steady state of constant activity, and presumably the coke also reached a pseudo-steady state of condensation.

3.2.2. H_2/CO_x feeds

Considering the aforementioned difference in catalyst deactivation for H_2 feed with CO and CO_2 (especially due to the higher H_2O generated with CO_2 *via* rWGS) is interesting to assess the differences among H_2/CO, H_2/CO/CO_2 and H_2/CO_2 feeds, although the lower reactivity of CO_2 in the methanol synthesis should be taken into account in the comparison.

Fig. 5 compares the evolution of CO_x conversion with time on stream for H_2/CO, H_2/CO_x (equimolar mixture of CO_2 and CO) and H_2/CO_2 feeds. Here, the difference in the initial deactivation rate was evident, in the order $H_2/CO > H_2/CO_x > H_2/CO_2$ and can be explained by the increase of the H_2O concentration in the medium with the presence of CO_2 in the feed (as it favors the greater extent of the rWGS) and its attenuating effect on coke formation. Moreover, this effect was also observed for different operating conditions (different In_2O_3-ZrO_2/SAPO-34 ratios, operating temperatures, pressures and space time values) (results not shown).

The yields obtained after 16 h on stream, i.e., at pseudo-steady state, are depicted in Fig. 6. The results were obtained with runs with CO_2/CO_x ratios in the feed of: 0, 0.25, 0.5, 0.75 and 1.

The maximum olefin yield value was achieved with a CO_2/CO_x ratio of 0.5, although the difference with the feeds with lower CO_2 amount was not remarkable. It is observed that, when increasing the CO_2 amount in the feed up to that value, the increase in H_2O concentration (as product of the rWGS reaction) enhanced the process by attenuating the deactivation. Indeed, with a CO_2/CO_x ratio of 0.5, in pseudo-steady state, SAPO-34 maintained a sufficient remaining activity for the complete conversion of oxygenates into olefins, avoiding their cracking into CH_4. The slight decrease of olefin yield for feeds with higher CO_2 content suggests that the effect of the lower reactivity of CO_2 with respect to CO [55] predominated over the expected higher attenuation of deactivation.

The effect of co-feeding H_2O and methanol together with H_2/CO_x on catalyst deactivation, for a CO_2/CO_x ratio of 0.5, was also studied. The results of evolution of the products with the time on stream revealed an

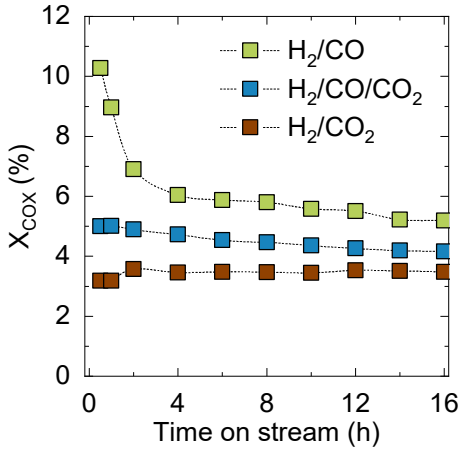

Fig. 5. Effect of CO_2/CO_x ratio in the feed (0, 0.5 and 1) on the evolution of CO_x conversion with time on stream. Reaction conditions: 400 °C; 30 bar; H_2/CO_x, 3; and space time, 5 g_{cat} h mol_C^{-1}.

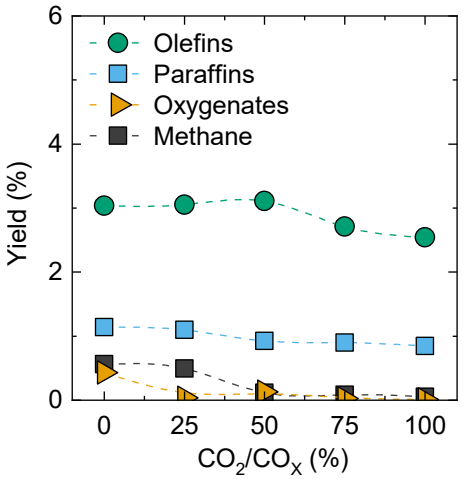

Fig. 6. Effect of CO_2/CO_x ratio in the feed on products yield. Reaction conditions: 400 °C; 30 bar; H_2/CO_x, 3; space time, 5 g_{cat} h mol_C^{-1}; and time on stream, 16 h.

intermediate trend to those observed previously for the H_2/CO and H_2/CO_2 feeds. Thus, the effect of co-feeding H_2O on the yields at the pseudo-steady state of the catalyst (Fig. 7) was in line with the aforementioned results. However, the unfavorable effects observed for the H_2/CO_2 feed predominated, due to the high H_2O concentration (generated by the rWGS reaction) that diminished the activity of the acid sites. According to this, H_2O co-feeding also inhibited olefin formation. On the other hand, the effect of increasing methanol concentration, especially without the compensation of co-feeding H_2O, was decisive to intensify the deactivation rate by coking, resulting in the inhibition of methanol conversion into olefins.

3.3. H_2/CO_x ratio in the feed

The effect of this variable was analyzed separately considering that, in addition to affecting the deactivation of the In_2O_3-ZrO_2/SAPO-34 tandem catalyst (leading to pseudo-steady states of different interest), it also affects directly the kinetics of the methanol/DME synthesis reactions. This direct effect will mask the results explained in the Section 3.2 about the concentration of H_2O and oxygenates.

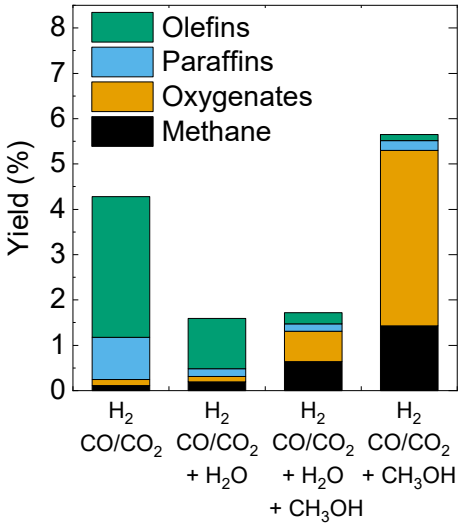

Fig. 7. Effect of different co-feedings on products yield. Reaction conditions: 400 °C; 30 bar; CO_2/CO_x, 0.5; H_2/CO_x, 3, 5 g_{cat} h mol_C^{-1}; space time, 5 g_{cat}h mol_C^{-1}; and time on stream, 16 h.

The results of the evolution of products yields with time on stream shown in Fig. 8 correspond to feeds with H_2/CO_x molar ratio of 1, 2 and 3 (Fig. 8a, 8b and 8c, respectively). It is evidenced that the higher H_2 partial pressure augmented the initial olefin yield, but also favored their hydrogenation into paraffins. Moreover, the catalyst deactivation was remarkably attenuated when increasing H_2 partial pressure due to the hydrogenation of coke precursors [31,38]. As a consequence, by increasing the H_2/CO_x ratio, the catalyst maintained a higher remaining activity in the pseudo-steady state and the CO_2 and CO_x conversions values were higher (Fig. 8d).

The attenuation of deactivation with increasing H_2 concentration may be attributed to the effect on the content and nature of coke in the SAPO-34 catalyst. In the TPO profiles gathered in Fig. 9, it is observed that at higher H_2/CO_x ratio, the coke content decreased. Furthermore, although the symmetry of the profiles evidenced the aforementioned uniformity of coke, the different extent of the evolution towards condensed structures is noteworthy. The effect of H_2/CO_x ratio in Fig. 9 is moderate because in all three conditions the partial pressure of H_2 was high enough to hydrogenate coke precursors [40], and consequently to difficult its condensation into polyaromatic structures. These hydrogenation reactions presumably are activated by the In_2O_3-ZrO_2 catalyst sites in contact with the SAPO-34 catalyst. It is noteworthy that the temperature corresponding to the maximum combustion rate in the TPO profiles was low (in the range of 450–500 °C), indicating relatively little condensed coke. Moreover, it should be noted that it was proved in a previous work that coke is partially eliminated by means of an inert gas stream [46]. These results are in good agreement with the literature of the MTO and DTO processes, in which the coke is relatively little condensed under usual conditions (atmospheric pressure) [30,35,56]. The increase in the H_2/CO_x ratio in the feed on coke content and nature led to the lower deactivation rate of the catalysts and its greater remaining activity in the pseudo-steady state in Fig. 8, due to the greater ease of the reactants to access the cages of the SAPO-34. Based on these results, an H_2/CO_x ratio above 3 could be considered adequate to further mitigate deactivation. However, H_2 availability must be considered to establish an optimal H_2/CO_x value. Accordingly, a value of 3 at 30 bar was set as appropriate, achieving a good compromise between olefin yield-selectivity and catalyst stability [41], bearing in mind that under

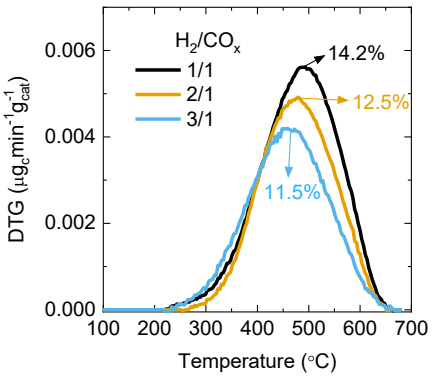

Fig. 9. Effect of H_2/CO_x ratio in the feed on the TPO profiles of spent SAPO-34 and the corresponding coke content (wt%). Reaction conditions: 400 °C; 30 bar; CO_2/CO_x, 0.5; space time, 5 g_{cat} h mol_C^{-1}, and; time on stream, 16 h.

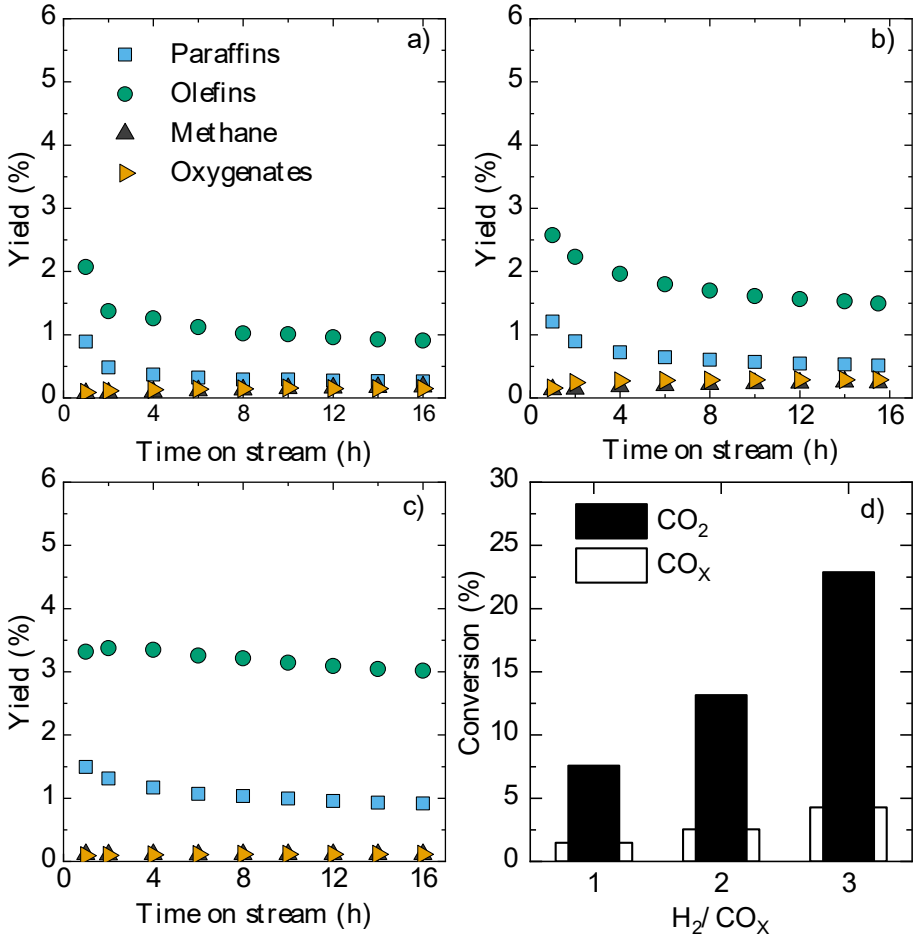

Fig. 8. Evolution of products yields with time on stream for H_2/CO_x values in the feed of 1 (a), 2 (b) and 3 (c), and CO_2 and COx conversion values at the pseudo-steady state of the catalyst (16 h on stream) (d). Reaction conditions: 400 °C; 30 bar; CO_2/CO_x 0.5, and; space time 5 g_{cat} h mol_C^{-1}.

these conditions H_2 produced with PEM electrolyzers could be used [57].

4. Conclusions

The rapid deactivation by coke of the SAPO-34 catalyst conditions the performance of the In_2O_3-ZrO_2/SAPO-34 tandem catalyst in the direct synthesis of olefins from CO_2/CO and the yield of olefins and byproducts (paraffins and CH_4) in the subsequent pseudo-steady state.

The increase in H_2 concentration resulted in lower coke deposition and of less condensed nature, which contributes to lessen de deactivation rate and to increase the remaining activity of the catalyst in the pseudo-steady state. However, the role of H_2O and oxygenates (methanol/DME) concentration on the deactivation of the SAPO-34 was complex, due to the implication of these compounds (reaction intermediates) in the mechanism of the main and deactivation reactions involved in the conversion of the oxygenates. Increasing H_2O concentration lessened the deactivation of the SAPO-34 catalyst for H_2/CO feed, boosting olefins yield. However, this did not occur for the H_2/CO_2 feed, because the H_2O concentration was too high at this condition, and its negative effect of attenuating the activity of the acid sites of the SAPO-34 predominated. In addition, the excessive concentration of methanol/DME, desired as reactants for olefin production, had the counterpart of favoring deactivation by coke, and consequently the presence of DME and CH_4 as by-products.

These effects of H_2O and methanol concentration affect the performance of the tandem In_2O_3-ZrO_2/SAPO-34 catalyst in the conversion to olefins of CO_2/CO mixtures, in which the H_2O concentration in the feed would also influence the effect of other operating conditions (temperature, pressure, space time, In_2O_3-ZrO_2/SAPO-34 ratio) on the deactivation. Consequently, when studying the effect of the process conditions for the interpretation of the results, their effect on the H_2O and oxygenates concentrations must be taken into account. Moreover, the incidence of H_2O and oxygenates concentrations should be taken into account in the development of kinetic models for this process, and in particular, in the kinetics of deactivation by coke. These effects are also of interest to progress in the design of new catalysts (more stable in the presence of H_2O and with lower coke deposition) and reactors. Among the initiatives to modify the acid zeotype, the modulation of the acid strength and the generation of hierarchical porous structures (with mesopores inside the crystals or agglomerating the zeotype in a matrix) may contribute to attenuate coke deposition. To minimize the attenuation of the activity by the concentration of H_2O, it would be reasonable to use less hydrophilic zeotypes and their incorporation into composites with H_2O adsorbing materials. From the perspective of improving the reactor, hydrophilic membrane reactors may be a good solution to avoid the unfavorable effect of excess H_2O with CO_2/CO feeds.

CRediT authorship contribution statement

A. Portillo: Conceptualization, Investigation, Writing – original draft, Writing – review & editing. **O. Parra:** Validation, Visualization, Writing – original draft, Writing – review & editing. **J. Ereña:** Project administration, Funding acquisition. **A.T. Aguayo:** Methodology, Resources, Supervision, Project administration, Funding acquisition. **J. Bilbao:** Conceptualization, Writing – original draft, Writing – review & editing, Project administration, Funding acquisition. **A. Ateka:** Conceptualization, Writing – original draft, Writing – review & editing.

Declaration of Competing Interest

The authors declare that they have no known competing financial interests or personal relationships that could have appeared to influence the work reported in this paper.

Data availability

The authors are unable or have chosen not to specify which data has been used.

Acknowledgements

This work has been carried out with the financial support of the Ministry of Science, Innovation and Universities of the Spanish Government (PID2019-108448RB-100); the Basque Government (Project IT1645-22), the European Regional Development Funds (ERDF) and the European Commission (HORIZON H2020-MSCA RISE-2018. Contract No. 823745). A. Portillo is grateful for the Ph.D. grant from the Ministry of Science, Innovation and Universities of the Spanish Government (BES2017-081135) and O. Parra is grateful for the PhD grant from the Basque Government (PRE_2021_1_0014). The authors thank for technical and human support provided by SGIker (UPV/EHU).

Appendix A. Supplementary data

Supplementary data to this article can be found online at https://doi.org/10.1016/j.fuel.2023.128298.

References

[1] Zhou W, Cheng K, Kang J, Zhou C, Subramanian V, Zhang Q, et al. New horizon in C1 chemistry: breaking the selectivity limitation in transformation of syngas and hydrogenation of CO_2 into hydrocarbon chemicals and fuels. Chem Soc Rev 2019; 48:3193–228. https://doi.org/10.1039/c8cs00502h.
[2] Ramirez A, Sarathy SM, Gascon J. CO_2 derived E-fuels: research trends, Misconceptions, and Future Directions. Trends Chem 2020;2:785–95. https://doi.org/10.1016/j.trechm.2020.07.005.
[3] Cui X, Zhuang Y, Dong H, Du J. Multi-criteria screening of carbon dioxide utilization products combined with process optimization and evaluation. Fuel 2022;328:125319. https://doi.org/10.1016/j.fuel.2022.125319.
[4] Cortazar M, Santamaria L, Lopez G, Alvarez J, Amutio M, Bilbao J, et al. Fe/olivine as primary catalyst in the biomass steam gasification in a fountain confined spouted bed reactor. J Ind Eng Chem 2021;99:364–79. https://doi.org/10.1016/j.jiec.2021.04.046.
[5] Landa L, Remiro A, de la Torre R, Aguado R, Bilbao J, Gayubo AG. Global vision from the thermodynamics of the effect of the bio-oil composition and the reforming strategies in the H_2 production and the energy requirement. Energy Convers Manag 2021;239:114181. https://doi.org/10.1016/j.enconman.2021.114181.
[6] Moreira R, Bimbela F, Gil-Lalaguna N, Sánchez JL, Portugal A. Clean syngas production by gasification of lignocellulosic char: State of the art and future prospects. J Ind Eng Chem 2021;101:1–20. https://doi.org/10.1016/j.jiec.2021.05.040.
[7] Rosha P, Rosha AK, Ibrahim H, Kumar S. Recent advances in biogas upgrading to value added products: A review. Int J Hydrogen Energy 2021;46:21318–37. https://doi.org/10.1016/j.ijhydene.2021.03.246.
[8] De S, Dokania A, Ramirez A, Gascon J. Advances in the design of heterogeneous catalysts and thermocatalytic processes for CO_2 utilization. ACS Catal 2020;10: 14147–85. https://doi.org/10.1021/acscatal.0c04273.
[9] Zhou Z, Gao P. Direct carbon dioxide hydrogenation to produce bulk chemicals and liquid fuels via heterogeneous catalysis, Chinese. J Catal 2022;43:2045–56. https://doi.org/10.1016/s1872-2067(22)64107-x.
[10] Saeidi S, Najari S, Hessel V, Wilson K, Keil FJ, Concepción P, et al. Recent advances in CO_2 hydrogenation to value-added products — Current challenges and future directions. Prog Energy Combust Sci 2021;85:100905. https://doi.org/10.1016/j.pecs.2021.100905.
[11] Sharma P, Sebastian J, Ghosh S, Creaser D, Olsson L. Recent advances in hydrogenation of CO_2 into hydrocarbons via methanol intermediate over heterogeneous catalysts, Catal. Sci Technol 2021;11:1665–97. https://doi.org/10.1039/d0cy01913e.
[12] Guo S, Wang H, Qin Z, Li Z, Wang G, Dong M, et al. Feasibility, limit, and suitable reaction conditions for the production of alcohols and hydrocarbons from CO and CO_2 through hydrogenation, a thermodynamic consideration. Ind Eng Chem Res 2022;61:17027–38. https://doi.org/10.1021/acs.iecr.2c02898.
[13] Wang G, Zeng L, Cao J, Liu F, Lin Q, Yi Y, et al. Highly selective conversion of CO_2 to hydrocarbons over composite catalysts of ZnO-ZrO_2 and SAPO-34. Microporous Mesoporous Mater 2019;284:133–40.
[14] Ticali P, Salusso D, Ahmad R, Ahoba-Sam C, Ramirez A, Shterk G, et al. CO_2 hydrogenation to methanol and hydrocarbons over bifunctional Zn-doped ZrO_2/zeolite catalysts, Catal. Sci Technol 2021;11:1249–68. https://doi.org/10.1039/d0cy01550d.
[15] Liu Z, Ni Y, Hu Z, Fu Y, Fang X, Jiang Q, et al. Insights into effects of ZrO_2 crystal phase on syngas-to-olefin conversion over ZnO/ZrO_2 and SAPO-34 composite

catalysts, Chinese. J Catal 2022;43:877–84. https://doi.org/10.1016/s1872-2067(21)63908-6.
[16] Numpilai T, Wattanakit C, Chareonpanich M, Limtrakul J, Witoon T. Optimization of synthesis condition for CO_2 hydrogenation to light olefins over In_2O_3 admixed with SAPO-34. Energy Convers Manag 2019;180:511–23. https://doi.org/10.1016/j.enconman.2018.11.011.
[17] Ghosh S, Olsson L, Creaser D. Methanol mediated direct CO_2 hydrogenation to hydrocarbons: Experimental and kinetic modeling study. Chem Eng J 2022;435:135090. https://doi.org/10.1016/j.cej.2022.135090.
[18] Wang S, Wang P, Qin Z, Yan W, Dong M, Li J, et al. Enhancement of light olefin production in CO_2 hydrogenation over In_2O_3-based oxide and SAPO-34 composite. J Catal 2020;391:459–70. https://doi.org/10.1016/j.jcat.2020.09.010.
[19] Dang S, Gao P, Liu Z, Chen X, Yang C, Wang H, et al. Role of zirconium in direct CO_2 hydrogenation to lower olefins on oxide/zeolite bifunctional catalysts. J Catal 2018;364:382–93. https://doi.org/10.1016/j.jcat.2018.06.010.
[20] Gao P, Dang S, Li S, Bu X, Liu Z, Qiu M, et al. Direct Production of lower olefins from CO_2 conversion via bifunctional catalysis. ACS Catal 2018;8:571–8. https://doi.org/10.1021/acscatal.7b02649.
[21] Tan L, Zhang P, Cui Y, Suzuki Y, Li H, Guo L, et al. Direct CO_2 hydrogenation to light olefins by suppressing CO by-product formation. Fuel Process Technol 2019;196:106174. https://doi.org/10.1016/j.fuproc.2019.106174.
[22] Dang S, Li S, Yang C, Chen X, Li X, Zhong L, et al. Selective transformation of CO_2 and H_2 into lower olefins over In_2O_3-$ZnZrO_x$/SAPO-34 bifunctional catalysts. ChemSusChem 2019;12:3582–91. https://doi.org/10.1002/cssc.201900958.
[23] Chen J, Wang X, Wu D, Zhang J, Ma Q, Gao X, et al. Hydrogenation of CO_2 to light olefins on CuZnZr@(Zn-)SAPO-34 catalysts: Strategy for product distribution. Fuel 2019;239:44–52. https://doi.org/10.1016/j.fuel.2018.10.148.
[24] Zhang W, Wang S, Guo S, Qin Z, Dong M, Fan W, et al. GamCrOx/H-SAPO-34(F), a highly efficient bifunctional catalyst for the direct conversion of CO_2 into ethene and propene. Fuel 2022;329:125475. https://doi.org/10.1016/j.fuel.2022.125475.
[25] Pérez-Uriarte P, Ateka A, Aguayo AT, Bilbao J. Comparison of HZSM-5 zeolite and SAPO (-18 and-34) based catalysts for the production of light olefins from DME. Catal Lett 2016;146:1892–902. https://doi.org/10.1007/s10562-016-1829-z.
[26] Luo M, Hu B, Mao G, Wang B. Trace compounds confined in SAPO-34 and a probable evolution route of coke in the MTO process. ACS Omega 2022;7:3277–83. https://doi.org/10.1021/acsomega.1c05336.
[27] Ibáñez M, Pérez-Uriarte P, Sánchez-Contador M, Cordero-Lanzac T, Aguayo AT, Bilbao J, et al. Nature and location of carbonaceous species in a composite HZSM-5 zeolite catalyst during the conversion of dimethyl ether into light olefins. Catalysts 2017;7:254. https://doi.org/10.3390/catal7090254.
[28] Müller S, Liu Y, Vishnuvarthan M, Sun X, Van Veen AC, Haller GL, et al. Coke formation and deactivation pathways on H-ZSM-5 in the conversion of methanol to olefins. J Catal 2015;325:48–59. https://doi.org/10.1016/j.jcat.2015.02.013.
[29] Pérez-Uriarte P, Gamero M, Ateka A, Díaz M, Aguayo AT, Bilbao J. Effect of the acidity of HZSM-5 zeolite and the binder in the DME transformation to olefins. Ind Eng Chem Res 2016;55:1513–21. https://doi.org/10.1021/acs.iecr.5b04477.
[30] Cordero-Lanzac T, Ateka A, Pérez-Uriarte P, Castaño P, Aguayo AT, Bilbao J. Insight into the deactivation and regeneration of HZSM-5 zeolite catalysts in the conversion of dimethyl ether to olefins. Ind Eng Chem Res 2018;57:13689–702. https://doi.org/10.1021/acs.iecr.8b03308.
[31] Zhao X, Li J, Tian P, Wang L, Li X, Lin S, et al. Achieving a superlong lifetime in the zeolite-catalyzed MTO reaction under high pressure: synergistic effect of hydrogen and water. ACS Catal 2019;9:3017–25. https://doi.org/10.1021/acscatal.8b04402.
[32] Tian P, Wei Y, Ye M, Liu Z. Methanol to olefins (MTO): From fundamentals to commercialization. ACS Catal 2015;5:1922–38. https://doi.org/10.1021/acscatal.5b00007.
[33] Cordero-Lanzac T, Aguayo AT, Gayubo AG, Bilbao J. Consideration of the activity distribution using the population balance theory for designing a dual fluidized bed reactor-regenerator system. Application to the MTO process. Chem Eng J 2021;405:126448. https://doi.org/10.1016/j.cej.2020.126448.
[34] Pérez-Uriarte P, Ateka A, Aguayo AT, Gayubo AG, Bilbao J. Kinetic model for the reaction of DME to olefins over a HZSM-5 zeolite catalyst. Chem Eng J 2016;302:801–10. https://doi.org/10.1016/j.cej.2016.05.096.
[35] Pérez-Uriarte P, Ateka A, Gayubo AG, Cordero-Lanzac T, Aguayo AT, Bilbao J. Deactivation kinetics for the conversion of dimethyl ether to olefins over a HZSM-5 zeolite catalyst. Chem Eng J 2017;311:367–77. https://doi.org/10.1016/j.cej.2016.11.104.
[36] Cordero-Lanzac T, Martínez C, Aguayo AT, Castaño P, Bilbao J, Corma A. Activation of n-pentane while prolonging HZSM-5 catalyst lifetime during its combined reaction with methanol or dimethyl ether. Catal Today 2022;383:320–9. https://doi.org/10.1016/j.cattod.2020.09.015.
[37] Arora SS, Nieskens DLS, Malek A, Bhan A. Lifetime improvement in methanol-to-olefins catalysis over chabazite materials by high-pressure H_2 co-feeds. Nat Catal 2018;1:666–72. https://doi.org/10.1038/s41929-018-0125-2.
[38] Xie J, Firth DS, Cordero-Lanzac T, Airi A, Negri C, Øien-Ødegaard S, et al. MAPO-18 catalysts for the methanol to olefins process: influence of catalyst acidity in a high-pressure syngas (CO and H_2) environment. ACS Catal 2022;12:1520–31. https://doi.org/10.1021/acscatal.1c04694.
[39] Arora SS, Shi Z, Bhan A. Mechanistic basis for effects of high-pressure H_2 cofeeds on methanol-to-hydrocarbons catalysis over zeolites. ACS Catal 2019;9:6407–14. https://doi.org/10.1021/acscatal.9b00969.
[40] Nieskens DLS, Lunn JD, Malek A. Understanding the enhanced lifetime of SAPO-34 in a direct syngas-to-hydrocarbons process. ACS Catal 2019;9:691–700. https://doi.org/10.1021/acscatal.8b03465.
[41] Portillo A, Ateka A, Ereña J, Aguayo AT, Bilbao J. Conditions for the joint conversion of CO_2 and syngas in the direct synthesis of light olefins using In_2O_3–ZrO_2/SAPO-34 catalyst. Ind Eng Chem Res 2022;2021:10365–76. https://doi.org/10.1021/acs.iecr.1c03556.
[42] Portillo A, Ateka A, Ereña J, Bilbao J, Aguayo AT. Role of Zr loading into In_2O_3 catalysts for the direct conversion of CO_2/CO mixtures into light olefins. J Environ Manage 2022;316:115329. https://doi.org/10.1016/j.jenvman.2022.115329.
[43] Gao J, Jia C, Liu B. Direct and selective hydrogenation of CO_2 to ethylene and propene by bifunctional catalysts, Catal. Sci Technol 2017;7:5602–7. https://doi.org/10.1039/c7cy01549f.
[44] Chen TY, Cao C, Chen TB, Ding X, Huang H, Shen L, et al. Unraveling highly tunable selectivity in CO_2 hydrogenation over bimetallic In-Zr Oxide catalysts. ACS Catal 2019;9:8785–97. https://doi.org/10.1021/acscatal.9b01869.
[45] Frei MS, Mondelli C, Cesarini A, Krumeich F, Hauert R, Stewart JA, et al. Role of zirconia in indium oxide-catalyzed CO_2 hydrogenation to methanol. ACS Catal 2020;10:1133–45. https://doi.org/10.1021/acscatal.9b03305.
[46] Portillo A, Ateka A, Ereña J, Bilbao J, Aguayo A. Alternative acid catalysts for the stable and selective direct conversion of CO2/CO mixtures into light olefins. Fuel Process. Technol. 2022;238:107513. https://doi.org/10.1016/j.fuproc.2022.107513.
[47] Aguayo AT, del Campo AES, Gayubo AG, Tarrío A, Bilbao J. Deactivation by coke of a catalyst based on a SAPO-34 in the transformation of methanol into olefins. J Chem Technol Biotechnol 1999;74:315–21. https://doi.org/10.1002/(sici)1097-4660(199904)74:4<315::aid-jctb34>3.0.co;2-g.
[48] Aguayo AT, Gayubo AG, Vivanco R, Olazar M, Bilbao J. Role of acidity and microporous structure in alternative catalysts for the transformation of methanol into olefins. Appl Catal A Gen 2005;283:197–207. https://doi.org/10.1016/j.apcata.2005.01.006.
[49] Chen J, Li J, Wei Y, Yuan C, Li B, Xu S, et al. Spatial confinement effects of cage-type SAPO molecular sieves on product distribution and coke formation in methanol-to-olefin reaction. Catal Commun 2014;46:36–40. https://doi.org/10.1016/j.catcom.2013.11.016.
[50] Gayubo AG, Aguayo AT, Sánchez Del Campo AE, Tarrío AM, Bilbao J. Kinetic modeling of methanol transformation into olefins on a SAPO-34 catalyst. Ind Eng Chem Res 2000;39:292–300. https://doi.org/10.1021/ie990188z.
[51] Zapater D, Lasobras J, Soler J, Herguido J, Menéndez M. Comparison of conventional and two-zone fluidized bed reactors for methanol to olefins. Effect of reaction conditions and the presence of water in the feed. Ind Eng Chem Res 2022;61:5757–65.
[52] Palomo J, Rodríguez-Cano MA, Berruezo-García J, Rodríguez-Mirasol J, Cordero T. Efficient methanol dehydration to DME and light hydrocarbons by submicrometric ZrO2-ZSM-5 fibrillar catalysts with a shell-like structure. Fuel 2022;315:123283. https://doi.org/10.1016/j.fuel.2022.123283.
[53] Pérez-Uriarte P, Ateka A, Gamero M, Aguayo AT, Bilbao J. Effect of the operating conditions in the transformation of DME to olefins over a HZSM-5 zeolite catalyst. Ind Eng Chem Res 2016;55:6569–78. https://doi.org/10.1021/acs.iecr.6b00627.
[54] Hemelsoet K, Van Der Mynsbrugge J, De Wispelaere K, Waroquier M, Van Speybroeck V. Unraveling the reaction mechanisms governing methanol-to-olefins catalysis by theory and experiment. ChemPhysChem 2013;14:1526–45. https://doi.org/10.1002/cphc.201201023.
[55] Nielsen ND, Jensen AD, Christensen JM. The roles of CO and CO_2 in high pressure methanol synthesis over Cu-based catalysts. J Catal 2021;393:324–34. https://doi.org/10.1016/j.jcat.2020.11.035.
[56] Gayubo AG, Aguayo AT, Alonso A, Bilbao J. Kinetic modeling of the methanol-to-olefins process on a silicoaluminophosphate (SAPO-18) catalyst by considering deactivation and the formation of individual olefins. Ind Eng Chem Res 2007;46:1981–9. https://doi.org/10.1021/ie061278o.
[57] Shaner MR, Atwater HA, Lewis NS, McFarland EW. A comparative technoeconomic analysis of renewable hydrogen production using solar energy. Energy Environ Sci 2016;9:2354–71.